Crystallization Kinetics of HNO_3/H_2O Films Representative of Polar Stratospheric Clouds

Robert T. Tisdale, Ann M. Middlebrook,† Anthony J. Prenni, and Margaret A. Tolbert*

CIRES and Department of Chemistry and Biochemistry, University of Colorado at Boulder, Boulder, Colorado 80309-0216

Received: August 8, 1996; In Final Form: January 7, 1997[⊗]

The crystallization of binary HNO_3/H_2O aerosols may be an important step in the formation of type Ia polar stratospheric clouds (PSCs). We have used Fourier transform infrared (FTIR) spectroscopy to probe the crystallization kinetics of supercooled 2:1 and 3:1 H_2O:HNO_3 films to nitric acid dihydrate (NAD) and trihydrate (NAT), respectively. Nitric acid/ice films were grown on a silicon substrate at temperatures near the glass point. The substrate was then warmed to a temperature above the glass point, and the crystallization of the film was measured using FTIR absorption spectroscopy. The temperature dependence of the crystallization rate was used to determine the activation energy for a nitrate ion to cross the liquid−solid phase boundary. The activation energies ranged from 22 to 41 kcal mol^{-1} for NAD crystallization at temperatures between 177 and 168 K and from 22 to 35 kcal mol^{-1} for α-NAT crystallization at temperatures between 171 and 161 K. In addition, activation energies at higher temperatures were derived from recent viscosity measurements obtained between 225 and 298 K. A parametrization was then developed to fit all of the activation energy data between 160 and 298 K. Finally, homogeneous nucleation calculations were performed using the temperature-dependent activation energies in conjunction with previous measurements of aerosol nucleation rates at 190-202 K to determine the freezing rates for HNO_3/H_2O particles over a wide temperature range. These calculations indicate that nucleation of NAD from supercooled 2:1 H_2O:HNO_3 aerosols is rapid at relevant stratospheric temperatures. Nucleation of α-NAT from supercooled 3:1 H_2O:HNO_3 aerosols could occur as rapidly as within 1 day, but the uncertainty in the interfacial energy used for α-NAT is large.

Introduction

Research conducted over the past several years has clearly shown that heterogeneous chemistry on polar stratospheric cloud (PSC) particles plays an important role in the ozone depletion observed in both the Arctic and the Antarctic.[1] Analysis of lidar observations of PSC particles indicates that some (denoted type Ia) have radii greater than 1 μm and are nonspherical, consistent with crystalline particles.[2] Although these particles have commonly been assumed to be nitric acid trihydrate (NAT), their composition is still unknown. Several additional possibilities have been suggested, including nitric acid dihydrate (NAD),[3] nitric acid pentahydrate,[4] and a mixed acid hydrate $H_2SO_4 \cdot HNO_3 \cdot 5H_2O$.[5]

Studies of possible type Ia PSC formation mechanisms may provide insight into their composition. For example, it has been suggested that NAT might nucleate on particles of sulfuric acid tetrahydrate (SAT); however, several studies have indicated that there is a high nucleation barrier for this process.[6−8] Tabazadeh et al.[9,10] and Carslaw et al.[11] have recently performed theoretical calculations which predict that the cooling of stratospheric sulfate aerosols results in the formation of supercooled ternary solution particles of $H_2SO_4/HNO_3/H_2O$. Upon further cooling, the particles become essentially binary liquid solutions with a composition of ∼4.5:1 H_2O:HNO_3. Recent work by Meilinger et al.[12] has suggested that, in a polydisperse ensemble of particles subjected to rapid temperature fluctuations, smaller particles may contain more HNO_3 because the larger particles reach equilibrium more slowly. This could result in particles with a composition of approximately 3:1 H_2O:HNO_3. It is not clear whether or not these aerosols will crystallize to form type Ia PSCs.

Homogeneous nucleation theory is frequently used to estimate nucleation times for particles in the atmosphere. Although it may not adequately represent the nucleation process, homogeneous nucleation theory can give insight into the various factors controlling nucleation. In this theory, the nucleation rate, J, is given by

$$J = n_c\left(\frac{kT}{h}\right)\exp\left(-\frac{\Delta g_a}{kT}\right)\exp\left(-\frac{\Delta G_c}{kT}\right) \qquad (1)$$

where n_c is the molecular concentration in the liquid phase, h is Planck's constant, k is the Boltzmann constant, T is the temperature, and Δg_a and ΔG_c are activation energy parameters.[13] The first, Δg_a, usually referred to as the "diffusion activation energy", is a measure of the energy barrier for nitrate ions to cross the liquid−solid phase boundary. The second term, ΔG_c, is a measure of the energy barrier for the formation of a crystalline nucleus large enough to grow spontaneously by the addition of one monomer. The activation energies for crossing the phase boundary and for spontaneous growth decrease and increase, respectively, with increasing temperature. This leads to a maximum nucleation rate at some intermediate temperature.

A previous study of aerosol crystallization in our laboratory has measured the nucleation rate, J, for NAD from a 2:1 H_2O:HNO_3 aerosol over the temperature range 193−204 K.[14] In the present study, we use Fourier transform infrared (FTIR) spectroscopy to monitor the crystallization of thin films of HNO_3/H_2O. By measuring the crystallization rate over a range of temperatures, we determine the temperature-dependent diffusion activation energy, Δg_a. We combine our low-temperature measurements of Δg_a with estimates of Δg_a from viscosity measurements at higher temperatures[15] to obtain a parametrization of Δg_a that is valid from ∼160 to 298 K. We then use these temperature-dependent values of Δg_a with previously measured J values to determine ΔG_c using eq 1. Finally,

† Now at National Oceanic and Atmospheric Administration, Boulder, CO.

⊗ Abstract published in *Advance ACS Abstracts,* February 15, 1997.

S1089-5639(96)02415-2 CCC: $14.00

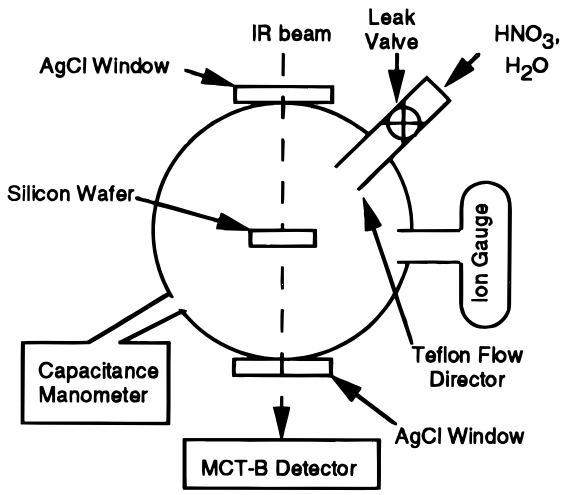

Figure 1. Schematic diagram of the experimental apparatus.

homogeneous nucleation theory is used to calculate the nucleation rates for NAD and NAT from supercooled HNO_3/H_2O aerosols over a wide temperature range.

Experimental Section

Apparatus. The vacuum chamber used to study the crystallization of film samples is shown schematically in Figure 1. Briefly, the HNO_3/H_2O films are condensed on a 1 mm thick silicon wafer held in place by a copper ring attached to a liquid nitrogen cryostat. A copper disk with a flexible Kapton heater is also in contact with the silicon wafer. Using this combination of liquid nitrogen cooling and resistive heating, the silicon wafer can be maintained at temperatures between 100 and 300 K. The temperature of the substrate was measured using type T thermocouple junctions in thermal contact with the silicon wafer. The temperature measurements were calibrated daily using the ice frost point as described by Iraci et al.[6] The experimentally determined frost points agreed with the thermocouple temperatures to within 2 K. Here we report our results using the corrected thermocouple temperatures.

The films were studied using single-pass transmission infrared spectroscopy. Collimated infrared light from a Nicolet Magna 550 FTIR spectrometer was focused into the chamber and onto the silicon wafer using a 90° off-axis parabolic mirror (6 in. effective focal length). Infrared light exiting the chamber was then refocused onto a liquid nitrogen cooled MCT-B detector using an ellipsoidal mirror. The external optics were enclosed in plexiglass boxes purged with dry, CO_2-free air. The infrared spectra presented here were collected using 4 cm^{-1} resolution with 8−64 scans coadded. Spectra were collected at regular intervals, ranging from once every 1.6 s to once every 19.2 s, until film crystallization was complete. Complete crystallization of supercooled 2:1 H_2O:HNO_3 films to NAD took approximately 30 s at 178 K and 41 min at 168 K. Complete crystallization of supercooled 3:1 H_2O:HNO_3 films to NAT took approximately 4 min at 171 K and 52 min at 161 K.

The infrared spectra for amorphous and crystalline 2:1 and 3:1 H_2O:HNO_3 films have been reported previously.[16−18] In this work, we use the previous infrared assignments in our analysis of the time-dependent film composition to derive the crystallization rates. Previous work has shown that there are two crystalline forms of NAT, denoted α-NAT and β-NAT. As in the earlier work,[17,18] we find that supercooled 3:1 H_2O:HNO_3 films first crystallize to α-NAT, with the conversion to β-NAT occurring at higher temperatures. In the current work, we restrict our discussion to α-NAT.

Film Growth. Films of 2:1 and 3:1 H_2O:HNO_3 were grown by directional dosing of HNO_3 and H_2O vapors onto one side of the cold silicon wafer using a Teflon flow director. Solutions of 65 and 63 wt % HNO_3 in H_2O at 0 °C provided the gas source for amorphous 2:1 and 3:1 H_2O:HNO_3 films, respectively. Although 65 and 63 wt % HNO_3 solutions at 0 °C would be expected to yield H_2O:HNO_3 gas ratios of 2.3:1 and 3.6:1, respectively,[19] differences in wall losses or evaporation rates for H_2O and HNO_3 may result in different vapor ratios in the chamber. The solution concentrations used were therefore determined empirically as those that formed amorphous films that crystallized to pure NAD and α-NAT, based on the infrared spectra. The solutions were purified using several freeze/pump/thaw cycles.

To grow amorphous films of a constant thickness, a leak valve between the solution bulb and the silicon wafer was opened, and the intensity of the FTIR spectrum was monitored with time. The leak valve was closed when the NO_3^- peak at 1300 cm^{-1} reached an absorbance of $A = 0.65 \pm 0.04$ absorbance units. After growth, the film thicknesses were determined using optical interference in the infrared region 4000−7000 cm^{-1}. Measured refractive indices[18] at the interference fringe maxima and minima were used according to the method of Moore.[20,21] Film thicknesses for amorphous 2:1 and 3:1 H_2O:HNO_3 were found to be 1.5 ± 0.1 μm and 1.7 ± 0.1 μm, respectively.

Films of 2:1 and 3:1 H_2O:HNO_3 were grown at 165 and 155 K, respectively. These temperatures are near the glass points of 161 K for NAD and between 149 and 160 K for NAT.[22] At temperatures above the glass points, the films are supercooled liquids which can crystallize. However, the crystallization rates are very slow at the growth temperatures. After growth, the films were heated to the desired crystallization temperature at a rate of approximately 1 K s^{-1}. Film crystallization was measured at a variety of temperatures between 160 and 180 K. The upper end of the temperature range was limited by the inability to warm the sample quickly enough to get to the target temperature before crystallization commenced. Desorption rates of the films were negligible compared to crystallization rates at the crystallization temperatures used. Even at the highest temperatures, an analysis of the infrared spectra revealed that less than 1% of the film desorbed during crystallization.

Results and Discussion

Experimental Determination of Crystallization Rates. Crystallization rates of the supercooled films were measured by monitoring the infrared spectra as a function of time at the desired crystallization temperature. Typical infrared spectra obtained during the crystallization of a supercooled film to α-NAT at 165 K are shown in Figure 2. The initial spectrum at 165 K appears to be that of amorphous 3:1 H_2O:HNO_3.[17,18] After 1.2 min, changes in the OH stretching region near 3400 cm^{-1} and the NO_3^- stretching region near 1400 cm^{-1} indicate the beginning of crystallization. By 10.8 min, the film has completely crystallized to α-NAT. Similarly, the infrared spectra of 2:1 H_2O:HNO_3 films show the evolution to crystalline NAD.

The infrared spectra were used to determine the fraction of the film remaining supercooled as a function of time. For α-NAT, the infrared peak at 3430 cm^{-1}, characteristic of an OH stretch in α-NAT, was used to calculate the fraction of the film that had crystallized. Because this peak appears on the shoulder of the broad OH peak, present in both amorphous and crystalline 3:1 films, it was baseline-corrected before being integrated from 3390 to 3460 cm^{-1}. The baseline-corrected integrations for each crystallization experiment were then

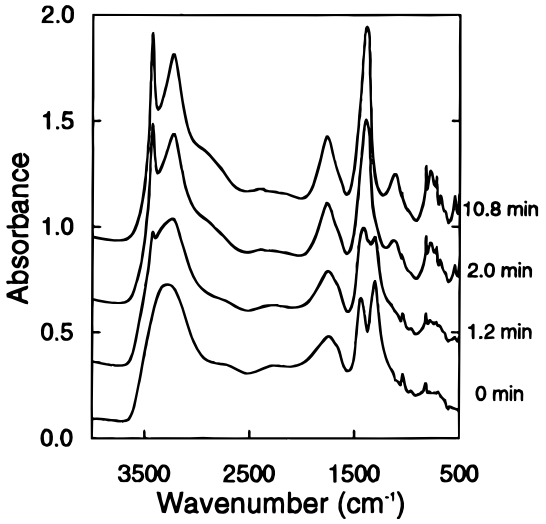

Figure 2. Infrared spectra of α-NAT film during crystallization at 165 K. For clarity, the spectra are offset by 0.3 absorbance units.

normalized, assuming that the minimum and maximum integrated absorbances corresponded to completely supercooled and fully crystallized films, respectively. The fraction of sample which remains supercooled, $F(t)$, is

$$F(t) = 1 - A_{3430}(t) \tag{2}$$

where $A_{3430}(t)$ is the normalized, baseline-corrected integrated area of the peak at 3430 cm^{-1}.

For NAD, peaks at 955 and 1040 cm^{-1} were used to calculate the fraction of the film remaining in the supercooled phase. This procedure has been described previously for work on aerosols.[14] The feature at 955 cm^{-1} is present in the spectrum of supercooled 2:1 H_2O:HNO_3 but absent in the spectrum of crystalline NAD. Thus, it is assumed that the mass in the supercooled phase, m_{sc} is proportional to the integrated area of the peak at 955 cm^{-1} (A_{955}). The peak at 1040 cm^{-1} is present in both spectra, and in supercooled 2:1 H_2O:HNO_3, the ratio $A_{1040}/A_{955} = 0.55$. This ratio differs from that reported by Disselkamp et al.,[14] which was obtained using a ratio of peak intensities rather than integrated areas. The mass of the sample crystallized, m_{NAD}, can be expressed as being proportional to the integrated area of the 1040 cm^{-1} peak minus the contribution from the mass remaining in the supercooled phase. Thus, $m_{NAD} \propto A_{1040} - (0.55)A_{955}$. The fraction of the sample in the supercooled phase as a function of time can then be written as

$$F(t) = \frac{m_{sc}}{m_{sc} + m_{NAD}} = \frac{A_{955}(t)}{A_{1040}(t) + 0.45(A_{955}(t))} \tag{3}$$

The fraction of film remaining in the supercooled phase as a function of time is shown in Figure 3 for the α-NAT case. Although data for only the first 1000 s are shown, all of the films eventually crystallized completely to α-NAT. The crystallization rates (fraction s^{-1}) were determined for each film by taking the time derivative of the crystalline fraction, $(1 - F(t))$, and are shown in Figure 4 for α-NAT. Both Figures 3 and 4 show that for all temperatures the crystallization rate increased with time, reached a maximum, and then decreased. Further, the maximum crystallization rate increased with increasing temperature. Finally, the time at which the maximum crystallization rate occurred decreased with increasing temperature. Similar behavior was observed for the crystallization of NAD, although at slightly higher temperatures.

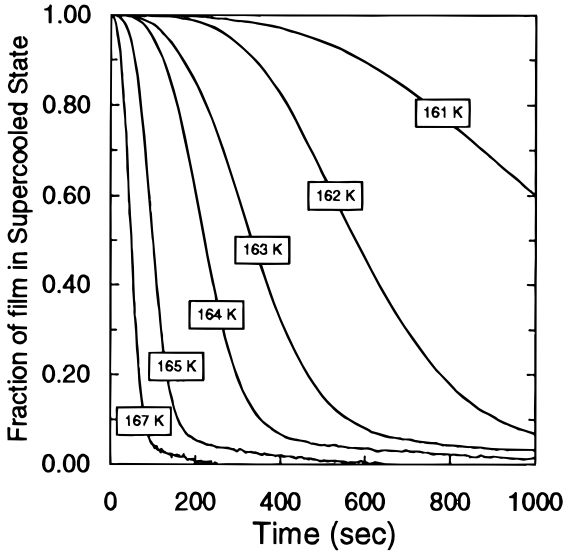

Figure 3. Fraction of the film in the supercooled phase as a function of time for 3:1 H_2O:HNO_3 at selected temperatures in the range studied.

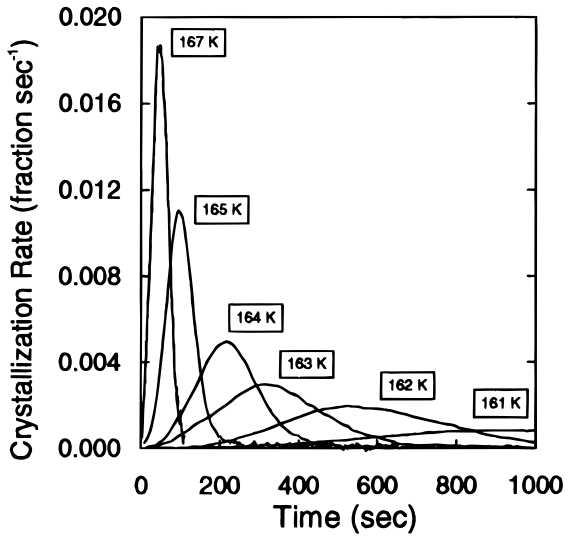

Figure 4. Rate of crystallization with time for 3:1 H_2O:HNO_3 at selected temperatures in the range studied.

Avrami Analysis of Crystallization Kinetics. The crystallization of thin films can be modeled using either the Avrami[23,24] or the Evans model.[25] These methods calculate the probability that crystallization has occurred at a particular location within the film given the expansion of crystallized volumes around randomly distributed nucleation sites. Both models lead to the following relationship between the supercooled fraction, F, and time, t:

$$F(t) = \exp(-Kt^n) \tag{4}$$

where K is a function of the nucleation site density and the crystallization velocity. The Avrami exponent, n, is dependent on the geometry of the system and the nucleation mechanism.[23−27] Unfortunately, conclusions about the nucleation and growth behavior during a phase transformation based on the Avrami exponent alone are tentative, as various interpretations exist for any given Avrami exponent.[25,26] In particular, different conclusions are possible if long-range diffusion is necessary for crystallization. However, in our study the supercooled films are nearly stoichiometric so that long-range diffusion should not limit crystallization. Despite the limitations, an Avrami−Evans analysis can provide some insight into the differences between the α-NAT and NAD crystallization mechanisms.

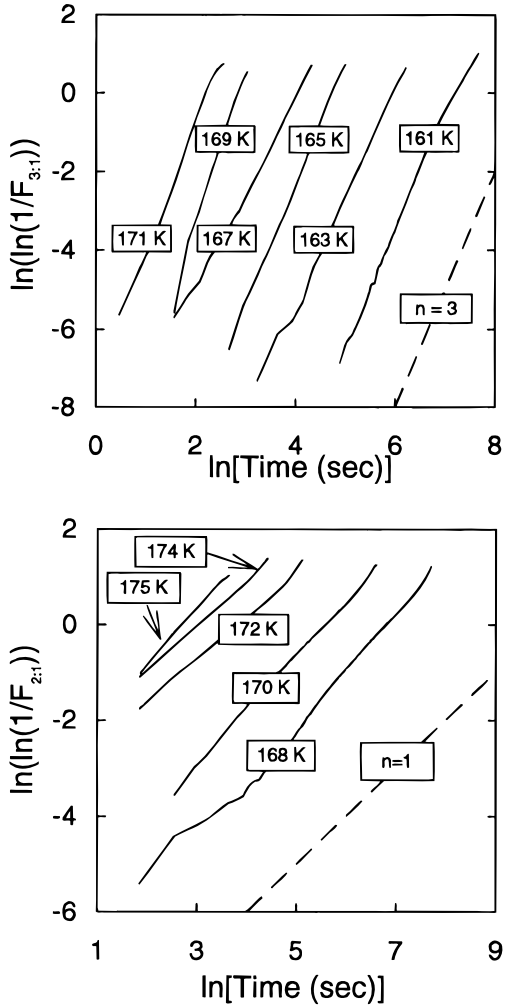

Figure 5. Avrami plots for (a, top) 3:1 H_2O:HNO_3 crystallizing to α-NAT and (b, bottom) 2:1 H_2O:HNO_3 crystallizing to NAD at several annealing temperatures in the range studied. The dashed lines have slopes of $n = 3$ and $n = 1$ and are included for reference.

The Avrami exponent is given by the slope of a plot of ln(ln(1/*F*)) versus ln(*t*). Figure 5a,b shows such plots for α-NAT and NAD crystallization, respectively. Fits (not shown) of the form given in eq 4 were also made to the data, allowing both *n* and *k* to vary freely. For α-NAT, *n* is approximately 3 over the temperature range from 161 to 171 K. According to the Avrami−Evans analysis, a value of $n = 3$ may be interpreted as nucleation occurring from a fixed distribution of nucleation sites which expand as overlapping spheres.[25,26] This seems reasonable for homogeneous nucleation in a 3-dimensional film with nucleation sites distributed throughout the film. However, it is also possible that 3-dimensional growth could occur from a heterogeneous surface with relatively few nucleation sites.

In contrast, *n* is approximately 1 for NAD crystallization at temperatures from 168 to 175 K. A value of $n = 1$ may be interpreted as linear growth from a fixed number of nuclei at a flat interface.[25,26] This type of crystal growth might be expected for a system with many nucleation sites at a heterogeneous surface. In this case, spherically expanding regions would quickly overlap to form a flat interface growing primarily in one dimension, perpendicular to the surface.

Although this analysis cannot yield unambiguous assignment of the crystallization mechanism, it is clear that the nucleation mechanisms for NAD and α-NAT in our system are quite different. In a study of the crystallization of 2:1 H_2O:HNO_3 aerosols to NAD between 190 and 202 K, Disselkamp et al.[14] also determined the Avrami exponent to be 1, consistent with our measurements. In addition, they found a low value for ΔG_c for NAD, favoring the formation of many critical nuclei. The agreement between these two experiments may be fortuitous. However, it is possible that heterogeneous nucleation occurred in both the 2:1 films and particles at the gas−liquid interface. In contrast, Disselkamp et al. did not observe nucleation of α-NAT aerosols.[14] As discussed below, this observation coupled with our measured values of Δg_a suggests a higher value of ΔG_c for α-NAT than for NAD. This would favor the formation of fewer critical nuclei for the α-NAT case. Thus, we might expect different crystallization kinetics for α-NAT and NAD based on differences in critical nucleus concentration. It is also possible that α-NAT crystallization occurs via homogeneous nucleation with critical nuclei dispersed throughout the film. Our Avrami−Evans kinetic analyses showing $n = 3$ for α-NAT and $n = 1$ for NAD are broadly consistent with either of these pictures.

Determination of the Activation Energy for the Transfer of NO_3^-. The temperature dependence of the crystallization rate can be used to determine the activation energy for the transfer of NO_3^- ions across the liquid−solid phase boundary. For films prepared at temperatures near the glass point and then heated, the limiting factor for crystallization should be transport of NO_3^- across the interface to the growing crystals. We thus assume that the temperature-dependent values of Δg_a can be obtained from an Arrhenius expression of the form

$$\Delta g_a = -k \frac{\delta(\ln(\mathrm{MCR}))}{\delta(1/T)} \tag{5}$$

where the maximum crystallization rate (MCR) is representative of the film crystallization rate. For eq 5 to hold, the surface area between the crystallized and supercooled phases must be constant at the MCR for any crystallization temperature, and the same number of critical nuclei must already be present for each α-NAT and NAD film, regardless of temperature. Because the films are all grown at low temperatures near the glass points, we believe that critical nuclei are present when the film reaches the crystallization temperature. Thus, each film should crystallize from the same number of critical nuclei, although the number may be different for α-NAT and NAD.

To test the assumption that the crystallizing film reaches the MCR at the same fraction supercooled, we calculated the expected F_{MCR} for the Avrami exponents $n = 3$ and $n = 1$. For $n = 3$, as is the case for 3:1 H_2O:HNO_3 films, this was done by setting the second derivative of eq 4 equal to zero, solving for the time when the MCR is reached, and then substituting that time into eq 4. The MCR should occur at $F_{MCR} = e^{-2/3} = 0.51$, in good agreement with the values of F_{MCR} between 0.47 and 0.55 from the fits to the crystallization data for the 3:1 films. For $n = 1$, as is the case for 2:1 H_2O:HNO_3, the MCR occurs at $F_{MCR} = 1$. The experimentally observed values of F_{MCR} ranged from 1.0 to 0.60 for the 2:1 films, in reasonable agreement with the expected value. Thus, the assumption that the MCR occurs at the same value of *F* seems to be valid for both α-NAT and NAD.

For each film, the MCR was determined from the best fits to the experimental data using eq 4. The ln(MCR) values from these fits are plotted as squares versus 1/*T* in Figure 6a,b for α-NAT and NAD, respectively. Because there were only a limited number of data points, a functional form of the temperature dependence of MCR was used to determine Δg_a in eq 5. The equation for the MCR was derived assuming that[28]

$$\mathrm{MCR} = ZT/\eta \tag{6}$$

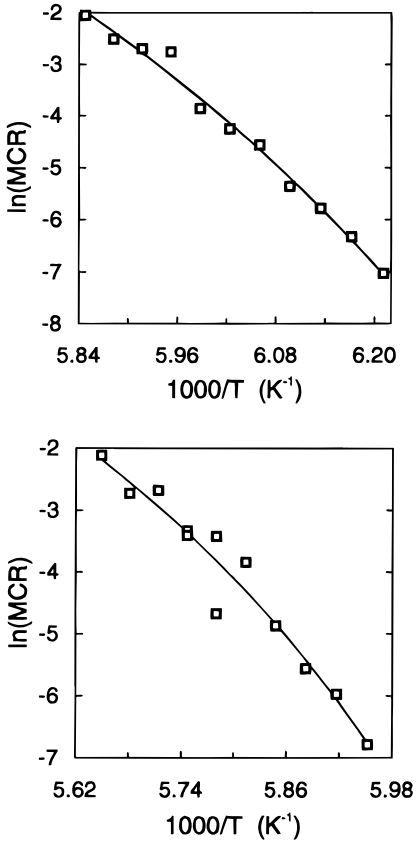

Figure 6. Arrhenius plots of the natural logarithm of the maximum crystallization rate versus $1/T$ for (a, top) 3:1 H_2O:HNO_3 and (b, bottom) 2:1 H_2O:HNO_3. The squares are the data points. The solid line is the fit to the data using eq 8.

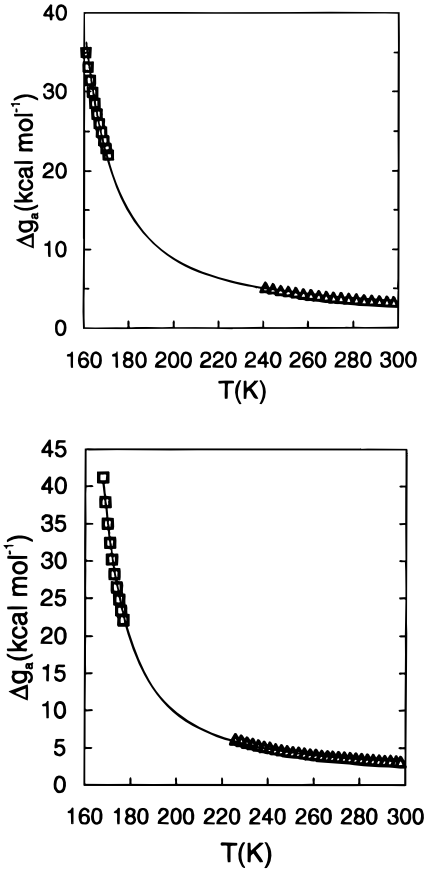

Figure 7. Diffusion activation energies for (a, top) 3:1 H_2O:HNO_3 and (b, bottom) 2:1 H_2O:HNO_3 calculated from this study (squares) and from viscosity measurements by Williams and Torok[15] (triangles). The solid lines are fits to the data using eq 9 and the parameters in Table 1. Note that the glass point for 3:1 H_2O:HNO_3 is between 149 and 160 K and for 2:1 H_2O:HNO_3 is 161 K.[22]

where Z is a constant and assuming a temperature-dependent viscosity, η, of the form[29]

$$\eta = A \exp\left(\frac{B}{T - T_0}\right) \tag{7}$$

where A, B, and T_0 are empirical parameters. This leads to the following equation used to fit the crystallization data:

$$\ln (\mathrm{MCR}) = \ln(A^*) + \ln(T) - \frac{B}{T - T_0} \tag{8}$$

where $A^* = Z/A$. The data in Figure 6 were fit using a nonlinear least-squares fitting program, and the fits are shown as curves.

The fits to the MCR data were used to derive values of Δg_a at each crystallization temperature for our films. Substitution of eq 8 into eq 5 yields

$$\Delta g_a = kT\left(1 + \frac{BT}{(T - T_0)^2}\right) \tag{9}$$

from which Δg_a was calculated. Our derived values of Δg_a, depicted as squares, are plotted as a function of temperature in Figure 7a,b for 3:1 and 2:1 H_2O:HNO_3, respectively. Both plots show that Δg_a increases with decreasing temperature. Both also show that Δg_a rises dramatically about 10 K above the glass point.

It was not possible to make measurements of Δg_a at polar stratospheric temperatures (~185−200 K) because the films crystallized too rapidly. We have thus calculated values of Δg_a using recent viscosity measurements made at temperatures between 241 and 298 K for 3:1 H_2O:HNO_3 and between 226 and 298 K for 2:1 H_2O:HNO_3.[15] This was done using the method described by Luo et al.[30] First, the "effective diffusion activation energy", Δg_{sol}, was determined with the Arrhenius relation[30]

$$\Delta g_{sol} = k \frac{\delta(\ln(\eta/T))}{\delta(1/T)} \tag{10}$$

using the viscosity parametrization from Williams and Torok.[15] The temperature dependence of Δg_a was assumed to have the same temperature dependence as Δg_{sol}:[30]

$$\Delta g_a(T) = \Delta g_a(T_1) \frac{\Delta g_{sol}(T)}{\Delta g_{sol}(T_1)} \tag{11}$$

where $T_1 = 298$ K and the value $\Delta g_a(T_1)$ was estimated from thermodynamic quantities as described in the Appendix.[31−35] The temperature-dependent values of Δg_a were calculated from the viscosity measurements using eqs 10 and 11 and are depicted as triangles in Figure 7a,b.

To calculate Δg_a over the range of stratospheric interest, Δg_a values from our crystallization rate data and from the viscosity data were fit to eq 9. These fits are shown as the solid lines in Figures 7a,b. The parameters for the fits are $B = 433.6$ K and $T_0 = 136.1$ K for α-NAT and $B = 335.1$ K and $T_0 = 146.3$ K for NAD. Note that the fits yield values of T_0 which are much lower than the measured glass points for α-NAT and NAD. This is in agreement with previous work which indicates that empirical fits to viscosity data yield values of T_0 which do not agree with experimentally measured glass points.[29] The fits

TABLE 1: Calculation of ΔG_c and σ from Disselkamp et al.[14] *J* Values

	T (K)	J (cm^{-3} s^{-1})	Δg_a (kcal mol^{-1})	ΔG_c (kcal mol^{-1})	σ (erg cm^{-2})
NAD	193	6.68×10^9	11.8	10.1	25.1
	200	1.54×10^9	9.6	13.6	24.4
	204	1.82×10^8	8.7	15.8	23.6
NAT	188	$<3.2 \times 10^7$	11.6	>11.5	>38.3

represent both the high temperature viscosity data and the low-temperature crystallization kinetics data extremely well. This gives us confidence in using the interpolated Δg_a values using eq 9, with the derived fit parameters, for stratospheric temperatures where no data are directly available from either method. The Δg_a values at polar stratospheric temperatures (185-200 K) range from 12.7 to 8.8 kcal mol^{-1} and from 15.6 to 9.6 kcal mol^{-1} for 3:1 and 2:1 H_2O:HNO_3, respectively.

Homogeneous Nucleation of α-NAT and NAD. The homogeneous freezing rate for atmospheric aerosols can be calculated theoretically using classical nucleation theory.[36] The expression for the homogeneous freezing rate, J (cm^{-3} s^{-1}), is given by eq 1, which can be rewritten as

$$J = n_c\left(\frac{kT}{h}\right)\exp\left(-\frac{\Delta g_a}{kN_AT}\right)\exp\left(-\frac{(16\pi/3)\sigma^3 N_A{}^2\upsilon^2}{kT\Delta H_f{}^2(\ln(T_m/T))^2}\right) \quad (12)$$

where n_c is the molecular concentration in the liquid phase, k is the Boltzmann constant, h is Planck's constant, σ is the interfacial surface energy between the solid and liquid phases, N_A is Avagadro's number, υ is the liquid volume per molecule, ΔH_f is the enthalpy of freezing, and T_m is the melting temperature. The values of n_c and υ can be estimated from density measurements of amorphous solid films of 2:1 H_2O:HNO_3 (1.52 g cm^{-3}) and 3:1 H_2O:HNO_3 (1.43 g cm^{-3}).[37] The values of ΔH_f and T_m are known from previous work; for NAD, ΔH_f = 20.15 kJ mol^{-1} and T_m = 235.5 K, and for α-NAT, ΔH_f = 29.11 kJ mol^{-1} and T_m = 255 K.[31,38,39]

The interfacial surface energy between 2:1 H_2O:HNO_3 and NAD has recently been measured as 24 erg cm^{-2} at 193 K by Disselkamp et al.[14] This value was arrived at using a value of 13.7 kcal mol^{-1} for Δg_a and a measured nucleation rate of $J = 6.68 \times 10^9$ cm^{-3} s^{-1}. However, at 193 K we find a somewhat lower value of Δg_a = 11.8 kcal mol^{-1} for 2:1 H_2O:HNO_3. We have thus recalculated the values of ΔG_c and σ for NAD using eqs 1 and 12 with Δg_a = 11.8 kcal mol^{-1}, yielding values of ΔG_c = 10.1 kcal mol^{-1} and σ = 25.1 erg cm^{-2} at 193 K. The values of ΔG_c and σ at 200 and 204 K were also recalculated using the J values measured by Disselkamp et al. and our present values of Δg_a. These recalculated ΔG_c and σ values are summarized in Table 1.

The interfacial energy for α-NAT has not been measured but has been estimated to have lower limits of 44.4 erg cm^{-2} at 192 K and 43.8 erg cm^{-2} at 190 K by MacKenzie et al.[7] Experiments conducted in our laboratory did not show crystallization of 1 μm diameter 3:1 H_2O:HNO_3 aerosols over a time period of 100 min at 188 K.[14,40] Assuming that 10% of the particles would need to freeze for detection, an upper limit of $J < 3.2 \times 10^7$ cm^{-3} s^{-1} can be placed on the α-NAT nucleation rate. Using this limit and our value of Δg_a = 11.6 kcal mol^{-1} for α-NAT at 188 K, we find that ΔG_c > 11.5 kcal mol^{-1} and σ > 38.3 erg cm^{-2} for α-NAT crystallizing from 3:1 H_2O:HNO_3, as shown in Table 1. This value of σ is broadly consistent with the estimated theoretical lower limits.[7]

Equation 12 can be used to explore the temperature dependence of α-NAT and NAD nucleation. One temperature-dependent term in this equation is Δg_a. Using the values of Δg_a and σ determined here, we have calculated homogeneous freezing rates for α-NAT and NAD over a range of temperatures, and the results are shown in Figure 8a,b, respectively. Two different J value curves are shown for α-NAT: one curve corresponding to the theoretical lower limit of σ = 43.8 erg cm^{-2} (solid line) and the other to the experimental lower limit of σ = 38.3 erg cm^{-2} (dotted line). For the NAD calculations, a constant value of σ = 25.1 erg cm^{-2} (solid line) and a temperature-dependent σ (dotted line), discussed below, were used. Also plotted for comparison are the values of J required for a 1 μm diameter particle to freeze in various time intervals, where $t = 1/(JV_p)$ and V_p is the particle volume. It should be noted that since the particle volume is proportional to the particle diameter cubed, changes in the particle size can have a profound effect on the time required for a particle to freeze.

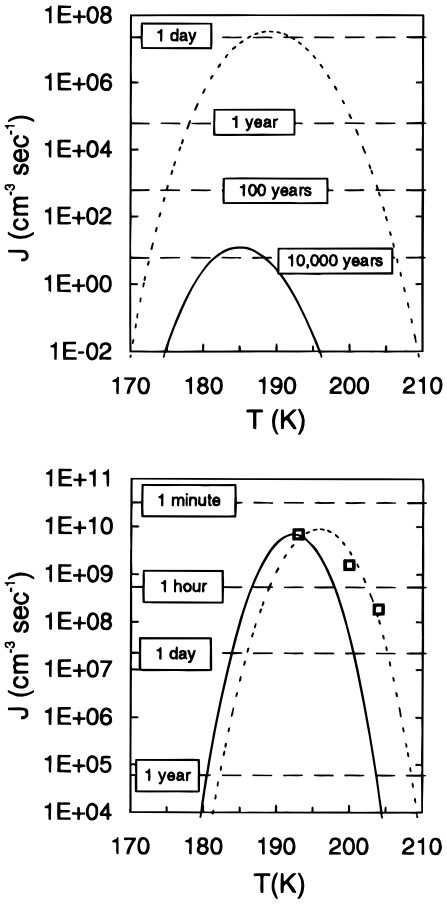

Figure 8. (a, top) Calculated J values for α-NAT assuming temperature-independent values of σ = 43.8 erg cm^{-2} (solid line) and σ = 38.3 erg cm^{-2} (dotted line). Also shown are the J values necessary for a 1 μm diameter particle to crystallize in the listed times (dashed horizontal lines). (b, bottom) Calculated J values for NAD assuming a temperature-independent value of σ = 25.1 erg cm^{-2} (solid line) and assuming a linear temperature dependence of σ (dotted line). Also shown are the measured J values from Disselkamp et al. (squares) and the J values necessary for a 1 μm diameter particle to crystallize in the listed times (dashed horizontal lines).

Figure 8b shows that 1 μm diameter 2:1 H_2O:HNO_3 particles are expected to freeze on a time scale of less than 1 h at temperatures between 187 and 197 K assuming a temperature-independent σ = 25.1 erg cm^{-2}. These results indicate that if a 2:1 H_2O:HNO_3 aerosol were able to form at stratospheric temperatures, NAD could rapidly crystallize. However, HNO_3 pressures in the stratosphere are normally too low to support formation of a 2:1 H_2O:HNO_3 aerosol.

In contrast, Figure 8a shows that the freezing time scale for α-NAT is much longer. The maximum freezing rate occurs at

approximately 189 and 184 K for the experimental and theoretical σ estimates, respectively. More importantly, the calculated lower limit for the freezing time of 3:1 H_2O:HNO_3 particles 1 μm in diameter is approximately 1 day between 186 and 192 K using the experimental σ estimate and over 5000 years at the same temperatures using the theoretical σ estimate. Since both the σ estimates are lower limits, the times for freezing in both cases are also lower limits. It is clear that small changes in the estimate of σ can result in enormous changes in the estimated freezing times for aerosols.

Meilinger et al. suggest that rapid temperature fluctuations at 190−195 K could result in the formation of 0.2-0.8 μm diameter particles composed of approximately 50 wt % HNO_3.[12] The estimated minimum freezing times calculated for 0.2 and 0.8 μm diameter particles of 3:1 H_2O:HNO_3 freezing to α-NAT at 190 K are ≥87 and ≥1.4 days, respectively, assuming that σ = 38.3 erg cm^{-2}. It is thus unclear whether such particles could crystallize during the time in which they are out of equilibrium with the rest of the aerosol. This analysis assumes that only particles of acid composition greater than roughly 50 wt % HNO_3 could freeze to α-NAT, which may be too restrictive. It is also possible that particles more dilute than 3:1 H_2O:HNO_3, expected to occur more commonly, could freeze to NAT.

One important limitation in the above analysis is that it was assumed that the interfacial surface energy in eq 12 was temperature independent. The temperature dependence of σ is often represented as a linear function:

$$\sigma(T) = \sigma_i + \omega(T - T_i) \tag{13}$$

where σ_i is the interfacial surface energy between the solid and liquid phases at some temperature, T_i. The temperature dependence of σ has been measured for several systems, including mercury,[41] gallium,[42] water,[43−45] and NaCl/water solutions.[43] All of these studies have observed that σ between the solid and liquid phases increases with increasing temperature, implying a positive value for ω. To our knowledge, a system in which σ decreases with increasing temperature has not been observed previously.

For NAD, our σ values yielded a linear fit with a negative value of ω. This temperature dependence of σ was then used to estimate the homogeneous freezing rate for 2:1 H_2O:HNO_3 aerosols as done above. The J values calculated for NAD in this way are shown as the dashed line in Figure 8b, with the Disselkamp et al.[14] data shown as squares. The estimated freezing rates using a temperature-dependent σ are very similar to those estimated using a constant σ, although the maximum freezing rate occurs at higher temperatures. The freezing time for 1 μm diameter aerosols is estimated to be less than an hour between 189 and 202 K.

The negative temperature dependence of σ may be explained by a thermodynamic model proposed by Spaepen.[46] This model relates the temperature dependence of σ to properties of a hypothetical "interface region" between the solid and liquid phases. The model uses the thickness of the interface region as well as the entropy and enthalpy changes in going from liquid to solid (ΔS_f and ΔH_f) and from liquid to the interface region (ΔS_i and ΔH_i). As pointed out by Spaepen, a positive temperature dependence of σ for mercury requires that ΔS_i is at least 50% of ΔS_f. Some examination of the model reveals that lower positive values or negative values of ΔS_i can lead to a negative temperature dependence of σ. The model was designed for use with elemental liquids and solids, however, so the assumptions in it may lead to errors when used for molecular liquids and solids.

To our knowledge, no studies of the temperature dependence of the interfacial surface energy between α-NAT and supercooled 3:1 H_2O:HNO_3 have been performed. As a result, we have done no calculations for α-NAT using a temperature-dependent σ, although it almost certainly has some temperature dependence. Additional nucleation experiments may provide insight into the temperature dependence of σ for ionic structured liquids such as the acidic solutions composing PSCs.

Finally, it is possible that other assumptions of homogeneous nucleation theory may be invalid, leading to the observed temperature trend in σ for NAD aerosols. If other parameters assumed to be temperature-independent vary with temperature, an incorrect temperature dependence of σ could be derived. In addition, some previous studies have shown that σ may exhibit a dependence on the droplet radius.[47,48] In a study of H_2O ice nucleation, Wood and Walton showed that this radius dependence could lead to an apparent temperature dependence capable of explaining the deviations of their experimental data from theory.[44] Wood and Walton also suggest that the theory itself may be flawed because highly structured liquids may nucleate by additions of molecular clusters rather than monomers in the formation of critical nuclei.

Conclusions

The diffusion activation energies have been determined for both 2:1 and 3:1 solutions of H_2O:HNO_3 at low temperatures using crystallization data and at high temperatures using viscosity measurements. Interpolation to stratospheric temperatures indicates that 2:1 solutions have a higher diffusion activation energy than 3:1 solutions at PSC temperatures. However, ΔG_c for NAD is substantially lower than for α-NAT. Together with measurements of other parameters used in homogeneous nucleation theory, the homogeneous freezing nucleation rates of binary 2:1 and 3:1 H_2O:HNO_3 solutions were estimated. These calculations indicate that if 1 μm diameter 2:1 H_2O:HNO_3 particles could form, NAD would homogeneously nucleate in less than 1 h at stratospheric temperatures. In contrast, α-NAT nucleation from 3:1 H_2O:HNO_3 solutions is calculated to be much slower. Using the experimental lower limit of σ, we calculate a NAT nucleation time of ≥1 day. However, the actual temperature dependencies of σ for both NAD and α-NAT are uncertain, and small changes in this dependence could produce large changes in the predicted homogeneous freezing nucleation rates. The possibility also exists that α-NAT particles could nucleate more rapidly from liquid particles with H_2O:HNO_3 ratios more dilute than 3:1. In addition, if suitable nuclei are available, the heterogeneous freezing rate of α-NAT from a 3:1 solution should be slightly greater than that of NAD from a 2:1 solution.

Acknowledgment. The authors are grateful to Leah Williams for providing us with measured viscosities of HNO_3/H_2O mixtures prior to publication. This work was supported by NSF (ATM-9321582) and NASA (SASS-94-091). R.T.T. was supported by a NASA Global Change Fellowship, A.M.M. was supported as a DOE Global Change Distinguished Postdoctoral Fellow, A.J.P. was supported by a CU/NSF Atmospheric Chemistry Fellowship, and M.A.T. was supported as an NSF Young Investigator and a Camille Dreyfus Teacher Scholar.

Appendix

Estimation of Δg_a at 298 K. The values of Δg_a at 298 K were estimated using the method of Luo et al.[30] It is assumed that Δg_a is composed of two parts. The first, Δg_a^{disp}, is the activation energy for moving the neighboring atoms and ions.

TABLE 2: Parameters Used To Calculate Δg_a at 298 K for 3:1 and 2:1 H_2O:HNO_3[a]

	3:1 H_2O:HNO_3	2:1 H_2O:HNO_3	ref
$\Delta g_a(100\%)$	2.41	2.41	32, eq 9
Δg_w^{bond}	1.60	1.60	33
$\Delta H_a(100\%)$	9.355	9.355	31
ΔH_w	10.52	10.52	34
Δg_a^{disp}	0.99	0.99	eq 15
$\Delta g_a^{bond}(100\%)$	1.41	1.41	eq 14
L_2(wt %)	−5.63	−4.45	35
ΔH_a(wt %)	14.98	13.81	31, 35
Δg_a(wt %)	3.30	3.10	eq 14

[a] All units are in kcal mol^{-1}.

This energy is assumed to be relatively constant with solution concentration. The second part, Δg_a^{bond}, is the activation energy for breakage of the hydrogen bonds of the moving ions. This energy does depend on solution concentration. It is further assumed that Δg_a^{bond} is approximately proportional to the partial heat of vaporization of nitric acid in solution, ΔH_a:

$$\Delta g_a(\text{wt \%}) \approx \Delta g_a^{disp} + \frac{\Delta H_a(\text{wt \%})}{\Delta H_a(100\%)} \Delta g_a^{bond}(100\%) \quad (14)$$

where 100% refers to pure HNO_3 and wt % refers to the HNO_3 weight percent in the 2:1 or 3:1 H_2O:HNO_3 solution. In addition, Δg_a can be expressed by

$$\Delta g_a(\text{wt \%}) \approx \Delta g_a^{disp} + \frac{\Delta H_a(\text{wt \%})}{\Delta H_w} \Delta g_w^{bond} \quad (15)$$

where ΔH_w is the heat of vaporization of water and Δg_w^{bond} is the activation energy for the breakage of the hydrogen bonds in water.

The following procedure was used to calculate Δg_a(wt %) at 298 K. First, the value of $\Delta g_a(100\%)$ was calculated by fitting viscosity data[32] for 100 wt % HNO_3 to eq 9. Using this value and the literature values for $\Delta H_a(100\%)$, ΔH_w, and Δg_w^{bond} given in Table 2, Δg_a^{disp} was calculated from eq 15. Next, $\Delta g_a^{bond}(100\%)$ was calculated using eq 14 and the above values of $\Delta g_a(100\%)$ and Δg_a^{disp}. Finally, to calculate the values of Δg_a(wt %) using eq 14, the values of ΔH_a(wt %) must be estimated. This was done by assuming that $\Delta H_a(\text{wt \%}) = \Delta H_a(100\%) - L_2(\text{wt \%})$, where L_2 is the partial mixing heat for HNO_3. The values used in our analysis are listed in Table 2.

References and Notes

(1) Solomon, S. *Rev. Geophys.* **1988**, *26*, 131.
(2) Toon, O. B.; Browell, E. V.; Kinne, S.; Jordan, J. *Geophys. Res. Lett.* **1990**, *17*, 393.
(3) Worsnop, D. R.; Fox, L. E.; Zahniser, M. S.; Wofsy, S. C. *Science* **1993**, *259*, 71.
(4) Marti, J. J.; Mauersberger, K. *J. Phys. Chem.* **1994**, *98*, 6897.
(5) Fox, L. E.; Worsnop, D. R.; Zahniser, M. S.; Wofsy, S. C. *Science* **1995**, *267*, 351.
(6) Iraci, L. T.; Middlebrook, A. M.; Tolbert, M. A. *J. Geophys. Res.* **1995**, *100*, 20969.
(7) MacKenzie, A. R.; Kulmala, M.; Laaksonen, A.; Vesala, T. *J. Geophys. Res.* **1995**, *100*, 11275.
(8) Molina, M. J.; Zhang, R.; Wooldridge, P. J.; McMahon, J. R.; Kim, J. E.; Chang, H. Y.; Beyer, K. D. *Science* **1993**, *261*, 1418.
(9) Tabazadeh, A.; Turco, R. P.; Jacobson, M. Z. *J. Geophys. Res.* **1994**, *99*, 12897.
(10) Tabazadeh, A.; Turco, R. P.; Drdla, K.; Jacobson, M. Z.; Toon, O. B. *Geophys. Res. Lett.* **1994**, *21*, 1619.
(11) Carslaw, K. S.; Luo, B. P.; Clegg, S. L.; Peter, T.; Brimblecombe, P.; Crutzen, P. J. *Geophys. Res. Lett.* **1994**, *21*, 2479.
(12) Meilinger, S. K.; Koop, T.; Luo, B. P.; Huthwelker, T.; Carslaw, K. S., Krieger, U.; Crutzen, P. J.; Peter, T. *Geophys. Res. Lett.* **1995**, *22*, 3031.
(13) Turnbull, D.; Fisher, J. C. *J. Chem. Phys.* **1949**, *17*, 71.
(14) Disselkamp, R. S.; Anthony, S. E.; Prenni, A. J.; Onasch, T. B.; Tolbert, M. A. *J. Phys. Chem.* **1996**, *100*, 9127.
(15) Williams, L.; Torok, E. Manuscript in preparation.
(16) Ritzhaupt, G.; Devlin, J. P. *J. Phys. Chem.* **1991**, *95*, 90.
(17) Koehler, B. G.; Middlebrook, A. M.; Tolbert, M. A. *J. Geophys. Res.* **1992**, *97*, 8065.
(18) Toon, O. B.; Tolbert, M. A.; Koehler, B. G.; Middlebrook, A. M.; Jordan, J. *J. Geophys. Res.* **1994**, *99*, 25631.
(19) Clavelin, J.; Mirabel, P. *J. Chim. Phys. Phys.-Chim. Biol.* **1979**, *76*, 533.
(20) Moss, T. S. *Optical Properties of Semi-Conductors*; Butterworths Scientific Publications: London, 1959.
(21) Moore, W. J. *Appl. Opt.* **1994**, *33*, 4164.
(22) Ji, K. Docteur de L'Universite de Paris VII, Paris, France, 1994.
(23) Avrami, M. *J. Chem. Phys.* **1939**, *7*, 1103.
(24) Avrami, M. *J. Chem. Phys.* **1940**, *8*, 212.
(25) Evans, U. R. *Trans. Faraday Soc.* **1945**, *41*, 365.
(26) Doremus, R. H. *Rates of Phase Transformations*; Academic Press: Orlando, FL, 1985.
(27) Tro, N. J.; Nishimura, A. M.; Haynes, D. R.; George, S. M. *Surf. Sci.* **1989**, *207*, L961.
(28) Glasstone, S.; Laidler, K. J.; Eyring, H. *The Theory of Rate Processes*; McGraw-Hill: New York, 1941.
(29) Eicher, L. D.; Zwoliniski, B. J. *J. Phys. Chem.* **1971**, *75*, 2016.
(30) Luo, B.; Peter, T.; Crutzen, P. *Geophys. Res. Lett.* **1994**, *21*, 1447.
(31) Forsythe, W. R.; Giauque, W. F. *J. Am. Chem. Soc.* **1942**, *64*, 48.
(32) Chanukvadze, O. P. *Zh. Obshch. Khim.* **1947**, *17*, 411.
(33) Gillen, K. T.; Douglass, D. C.; Hoch, J. R. *J. Chem. Phys.* **1972**, *57*, 5117.
(34) Gmitro, J. I.; Vermeulen, T. *AIChE J.* **1964**, *10*, 740.
(35) Clegg, S. L.; Brimblecombe, P. *J. Phys. Chem.* **1990**, *94*, 5369.
(36) Turnbull, D. *J. Chem. Phys.* **1950**, *18*, 198.
(37) Middlebrook, A. M.; Berland, B. S.; George, S. M.; Tolbert, M. A.; Toon, O. B. *J. Geophys. Res.* **1994**, *99*, 25655.
(38) Wooldridge, P. J., Zhang, R., Molina, M. J. *J. Geophys. Res.* **1995**, *100*, 1389.
(39) Ji, K.; Petit, J. C.; Négrier, P.; Haget, Y. *Geophys. Res. Lett.* **1996**, *23*, 981.
(40) Prenni, A. Personal communication, 1996.
(41) Turnbull, D. *J. Chem. Phys.* **1952**, *20*, 411.
(42) Miyazawa, Y.; Pound, G. M. *J. Cryst. Growth* **1974**, *23*, 45.
(43) Wood, G. R. Kinetics of Ice Nucleation from Water and Electrolyte Solutions, United States Department of the Interior, Office of Saline Water, Report No. 500, 1969.
(44) Wood, G. R.; Walton, A. G. *J. Appl. Phys.* **1970**, *41*, 3027.
(45) Huang, J.; Bartell, L. S. *J. Phys. Chem.* **1995**, *99*, 3924.
(46) Spaepen, F. *Solid State Phys.* **1994**, *47*, 1.
(47) Tolman, R. C. *J. Chem. Phys.* **1949**, *17*, 333.
(48) Kirkwood, J. G.; Buff, F. P. *J. Chem. Phys.* **1949**, *17*, 338.